



1 **The UNAM-MARine Aerosol Tank (UNAM-MARAT): An Evaluation of the**
2 **Ice-Nucleating Abilities of seawater from the Gulf of Mexico and the Mexican**
3 **Pacific**

4 M. Fernanda Córdoba¹, Rachel Chang², Harry Alvarez-Ospina³, Aramis Olivos⁴ Graciela
5 B. Raga¹, Daniel Rosas-Ramírez⁵, Guadalupe Campos⁶, Isabel Márquez³, Telma Castro¹,
6 and Luis A. Ladino^{1,*}

7 ¹Instituto de Ciencias de la Atmósfera y Cambio Climático, Universidad Nacional
8 Autónoma de México, Ciudad de México, C.P. 04510, México

9 ²Department of Physics and Atmospheric Science, Dalhousie University, C.P. B3H 4R2,
10 Canada

11 ³Facultad de Ciencias, Universidad Nacional Autónoma de México, México City, México

12 ⁴Centro Universitario de Investigaciones Oceanológicas, Universidad de Colima, C.P.
13 28860, México

14 ⁵Departamento de Química de Biomacromoléculas, Instituto de Química, Universidad
15 Nacional Autónoma de México, Av. Universidad 3000, Circuito Exterior S/N, Coyoacán,
16 Ciudad Universitaria, Mexico City, 04510, México

17 ⁶Laboratorio de Alimento Vivo, Procuraduría Estatal de Protección al Medio Ambiente-
18 Aquarium del Puerto de Veracruz, Blvd. Manuel Ávila Camacho s/n, Col. Ricardo Flores
19 Magón, C.P. 91900. Veracruz, Veracruz, México

20
21 *Corresponding author: luis.ladino@atmosfera.unam.mx

22 Keywords: Ice Nucleating Particles, Sea Spray, Mexican Pacific Ocean, Gulf of Mexico.

23 **Abstract**

24 Although several studies have shown that sea spray aerosol (SSA) has the potential to act as
25 ice nucleating particles (INP) impacting cloud formation, there is a lack of marine INP studies
26 in tropical latitudes. This is partly due to the unavailability of local oceanographic cruises
27 that perform aerosol-cloud interaction studies in the tropics, as well as the scarcity of
28 appropriate aerosol and cloud microphysics instrumentation. The present study shows the
29 development of the UNAM-MARine Aerosol Tank (UNAM-MARAT), a device that
30 simulates wave breaking to generate SSA particles with the main purpose to characterize
31 their physicochemical properties including their ice nucleating abilities. The UNAM-
32 MARAT was characterized using Instant Ocean Sea Salt and its potential to study ambient
33 sea waters was evaluated with sea seawater samples collected from the Port of Veracruz
34 (PoV) in the Gulf of Mexico, and from the Bay of Acapulco (BoA) and the Bay of Santiago-



35 Manzanillo (BoSM) in the Mexican Pacific Ocean. The portable and automatic UNAM-
36 MARAT is able to generate aerosol particle concentrations as high as 2000 cm^{-3} covering a
37 wide range of sizes, from 30 nm to $10 \mu\text{m}$, similar to those found in the ambient marine
38 boundary layer. The SSA generated from the three natural seawater samples was found to act
39 as INP via immersion freezing, with INP concentrations as high as 130.7 L^{-1} . The particles
40 generated from the BoA seawater samples were the most efficient INPs, reporting the highest
41 ice active site density (n_s) values between -20 and -30°C . Our results also show the direct
42 relationship between particle size and its composition. Larger particles ($> 1 \mu\text{m}$) were found
43 to be enriched in sodium chloride. In contrast, the fraction of Ca^{2+} , Mg^{2+} , and NO_3^- was found
44 to increase with decreasing the particle size from $10 \mu\text{m}$ to 320 nm. This suggests the
45 presence of dissolved organic material in the submicron particles.

46 **1 Introduction**

47 Sea-Spray Aerosol (SSA) is ubiquitous in oceanic regions and forms via bubble bursting by
48 wave breaking (Lamarre and Melville, 1991). It has been shown that SSA has the potential
49 to impact the Earth's radiative balance (Jacobson, 2001) and the hydrological cycle given
50 its capability to act as cloud condensation nuclei (CCN, Albrecht, 1989) and ice nucleating
51 particles (INP, Boucher et al., 2013; Vergara-Temprado et al., 2017; McCluskey et al.,
52 2018).

53 Laboratory experiments with diverse setups, including atomizers, nebulizers, and tanks (in
54 acrylic, PTFE or stainless steel), to simulate SSA generation via bubble bursting, have been
55 essential in determining the physicochemical and biological properties of SSA (Fuentes et
56 al., 2010; McCluskey et al., 2017; Christiansen et al., 2019; Wolf et al., 2020). Some of these
57 setups used different mechanisms for bubble production such as diffusers, glass frits or
58 systems like plunging-water jet or sheetlike (Cipriano & Blanchard, 1981; Fuentes et al.,
59 2010; Prather et al., 2013; Stokes et al., 2013; Christiansen et al., 2019). Using a small tank
60 to produce SSA, Cipriano & Blanchard (1981) determined that bubbles with diameter > 1
61 mm can produce aerosol particles $< 5 \mu\text{m}$ in diameter, while bubbles < 1 mm generate aerosol
62 particles $> 20 \mu\text{m}$. However, it is currently believed that submicron ($< 1 \mu\text{m}$) and supermicron
63 ($> 1 \mu\text{m}$) aerosol particles can be generated by the film drop and jet drop mechanisms,
64 respectively (Resch & Afeti, 1992; Lewis & Schwartz, 2004; Burrows et al., 2014).
65 Recently, Wang et al. (2017) found that the jet drop mechanism can produce up to 43% of
66 submicron SSA.

67 Results from field measurements and laboratory experiments indicate that SSA exhibits a
68 trimodal particle size distribution (PSD) with peaks observed at $0.02 - 0.05 \mu\text{m}$, $0.1 - 0.2$
69 μm , and $2 - 3 \mu\text{m}$ (Quinn et al., 2015). Laboratory experiments using artificial seawater in a
70 30 L marine aerosol tank, Sellegrì et al. (2006) demonstrated that the trimodal PSD of the
71 SSA can vary with other environmental variables such as sea surface temperature (SST). The
72 authors found that if SST decreases the peaks of the PSD are displaced towards smaller



73 diameters. The presence of surfactants (e.g., sodium dodecyl sulphate, SDS) can also
74 influence in the amplitude of the modal peaks as surfactants extend the bubble lifetime at the
75 surface, and then bubbles can be broken by wind or subsequent waves (Sellegri et al., 2006).
76 Additionally, Hartery et al. (2022) found that adding sodium dodecyl benzene sulfonate,
77 (SDBS, a surfactant) to a NaCl solution in the Dalhousie Automated Wave Tank (DAWT)
78 reduced particle size mode, particle concentration, and hygroscopicity, further highlighting
79 the impact of surfactants on aerosol properties. Using a similar experimental setup to the one
80 used by Sellegri et al. (2006), Fuentes et al. (2010) found that the SSA submicron size
81 distribution, its hygroscopicity, and its ability to act as CCN are not significantly affected by
82 the bubble bursting generation mechanism (i.e., porous bubblers and plunging- water jet
83 systems). Nevertheless, Fuentes et al. (2010) reported that the best system for SSA generation
84 when using natural sea water was the plunging-water jet, which improves the reproduction
85 of organic enrichment and PSD.

86 Stokes et al. (2013) implemented a new system for SSA generation that includes an
87 intermittent plunging sheet of water in a plexiglass 210 L tank, called the Marine Aerosol
88 Reference Tank (MART). This mechanism simulates the gravitational impingement of a
89 waterfall and the intermittence better reproduces wave breaking to create turbulence, the
90 bubble plumes, and foam formation. The interaction of freshly emitted SSA with volatile
91 organic compounds present in the marine atmosphere has been evaluated in the MART.
92 Trueblood et al. (2019) discovered that by exposing supermicron SSA to hydroxyl radicals
93 (OH), a fragmentation of the nitrogen-rich species (e.g., amino sugars or amino acids) is
94 observed, and therefore, there is a reduction in the organic matter present in the SSA.

95 In addition to the above-mentioned laboratory tanks, a large-scale experimental setup such
96 as the Wave Channel have provided insights into SSA generation under realistic marine
97 conditions. A large tank (33 m x 0.5 m x 1 m) was designed in the Hydraulics Laboratory at
98 the Scripps Institution of Oceanography (SIO) in San Diego – United States (Collins et al.,
99 2014). SSA is generated through a hydraulic-paddle- created waves, sintered glass filters,
100 and an intermittent plunging sheet of water (Collins et al., 2014). Simulation of ocean
101 dynamics and biological activity in the wave channel allowed Prather et al. (2013) to
102 conclude that SSA is composed mainly of four types of particles: sea salt (SS), sea salt with
103 organic carbon (SS-OC), organic carbon (OC), and biological (Bio) particles, with its
104 chemical composition strongly linked to particle size. The authors reported that supermicron
105 particles were dominated by SS and Bio, while submicron particles by SS-OC and OC.
106 Prather et al. (2013) also reported that Na, Cl, Mg, and K largely contribute to the SS particles
107 and that between 30 and 40% (v/v) of the SS-OC particles, correspond to organic matter. Ca
108 and Mg were found to be present in the OC particles, and they are known to be able to form
109 complexes with natural organic ligands (Quinn et al., 2015). Organic matter can accumulate
110 in the air-ocean interface, forming a gel-like layer with properties that differ from the
111 underlying waters. This layer, known as the sea surface microlayer (SML), has a typical



112 thickness that varies between 1 and 1000 μm (Wurl et al., 2017). In an experiment similar to
113 that carried out in the wave channel by Prather et al. (2013), Wang et al. (2015) determined
114 that marine submicron particles are enriched in aliphatic organic material and that the soluble
115 oxidized organic compounds are found in supermicron particles. Additionally, Wang et al.
116 (2015) showed that differences in the SSA chemical composition could result from a variety
117 of biological processes, including bacterial activity and phytoplankton primary production.

118 It is well known that SSA can act as an INP (Bigg, 1973; Schnell & Vali, 1975; Schnell,
119 1977; Rosinski et al., 1987; Rosinski et al., 1988; Wilson et al., 2015; McCluskey et al.,
120 2018). Several studies have suggested that marine biological particles are able to nucleate ice
121 such as the *Heterocapsa niei* (dinoflagellate) (Fall and Schnell, 1985) and *Thalassiosira*
122 *pseudonana* (diatom, Knopf et al., 2011; Alpert et al., 2011; Wilson et al., 2015). Through
123 controlled laboratory experiments in the MART, DeMott et al. (2016) demonstrated that the
124 INP number concentrations from seawater collected close to SIO - Pacific Ocean off the
125 California coast, are within the range reported by previous studies in different maritime
126 regions (Bigg, 1973; Schnell, 1977; Rosinski et al., 1988). However, the INP concentrations
127 were lower than the corresponding concentrations in the surface boundary layer over
128 continental regions. DeMott et al. (2016) also noted that the INP concentrations at -26 and -
129 30°C were a factor of 50 larger after nutrient addition than freshly collected seawater. Wang
130 et al. (2015) found that maximum concentrations of INP at $\geq -15^\circ\text{C}$ coincided with the peaks
131 of the phytoplankton bloom carried out in the wave channel. These experiments used
132 seawater from the Pacific Ocean near the SIO, suggesting that the observed ability to act as
133 INP could be due to amphiphilic long-chain alcohols monolayer and that the ice nucleating
134 activity (INA) was reduced when the samples went through the heating test, a process to
135 denature biological INP (Hill et al., 2016). McCluskey et al. (2017) used seawater collected
136 from the Pacific Ocean at the end of Scripps Pier (32°49'58.12" N, -117°16'16.58" W) in the
137 MART. Their study suggests that microorganisms and biomolecules contribute to the INP
138 population due to an increase of organic compounds during high INP concentrations.

139 Studies on INPs along the Mexican coasts and oceans are scarce. A pioneering study by
140 Rosinski et al. (1988) in the Gulf of Mexico (GoM) demonstrated that the efficiency of
141 aerosol particles as INP varies depending on their size, season, and sampling location. The
142 influence of environmental conditions on the ice nucleation efficiency of marine aerosol
143 particles was also evidenced by Ladino et al. (2019) and Córdoba et al. (2021). Both studies
144 found that the arrival of cold air masses to the Yucatan Peninsula (Mexico) from higher
145 latitudes increased the INP concentrations with aerosol particles capable to nucleate ice at -
146 3°C. The warm freezing temperature suggests the influence of biological material, likely
147 linked to bacteria and fungi from terrestrial and/or marine sources. Although the analyzed
148 samples were not airborne particles, Ladino et al. (2022) found that the sea subsurface water
149 (SSW) samples from the GoM exhibited better ice nucleation abilities than the sea surface
150 microlayer (SML) samples, contrary to the findings of Wilson et al. (2015) at higher



151 latitudes. This discrepancy could be attributed to a lower organic material content in the SML
152 samples of the GoM compared to those analyzed by Wilson et al. (2015). This difference in
153 nucleation efficiency was also associated with low phytoplankton concentrations during the
154 sampling period in the GoM, a crucial variable in the efficiency of particles as INPs.

155 Investigating SSA's role in marine environments is imperative for improving the accuracy of
156 climate predictions (Burrows et al., 2022). Given that SSA ability to act as INP varies
157 spatially and temporally (Burrows et al., 2013; Wilson et al., 2015; DeMott et al., 2016) and
158 the scarcity of ice nucleation studies in tropical latitudes over maritime regions (Rosinski et
159 al., 1988; Yakobi-Hancock et al., 2014; Wolf et al., 2020; Córdoba et al., 2021; Ladino et al.,
160 2022; Melchum et al., 2023), expanding research efforts to study unexplored regions, such
161 as the Mexican coasts, is of high importance. By advancing our understanding of SSA
162 dynamics, we can enhance the accuracy of atmospheric models and reduce the uncertainties
163 associated with aerosol-cloud interactions, thereby, contributing to more robust climate
164 projections. The present study involves the building and characterization of a new device to
165 generate SSA by simulating wave breaking through the intermittent plunging sheet of water
166 mechanism, utilizing water samples from seawater collected offshore the Mexican coasts.

167 **2 Instrument development**

168 **2.1 Description and Operation of the UNAM-MARAT**

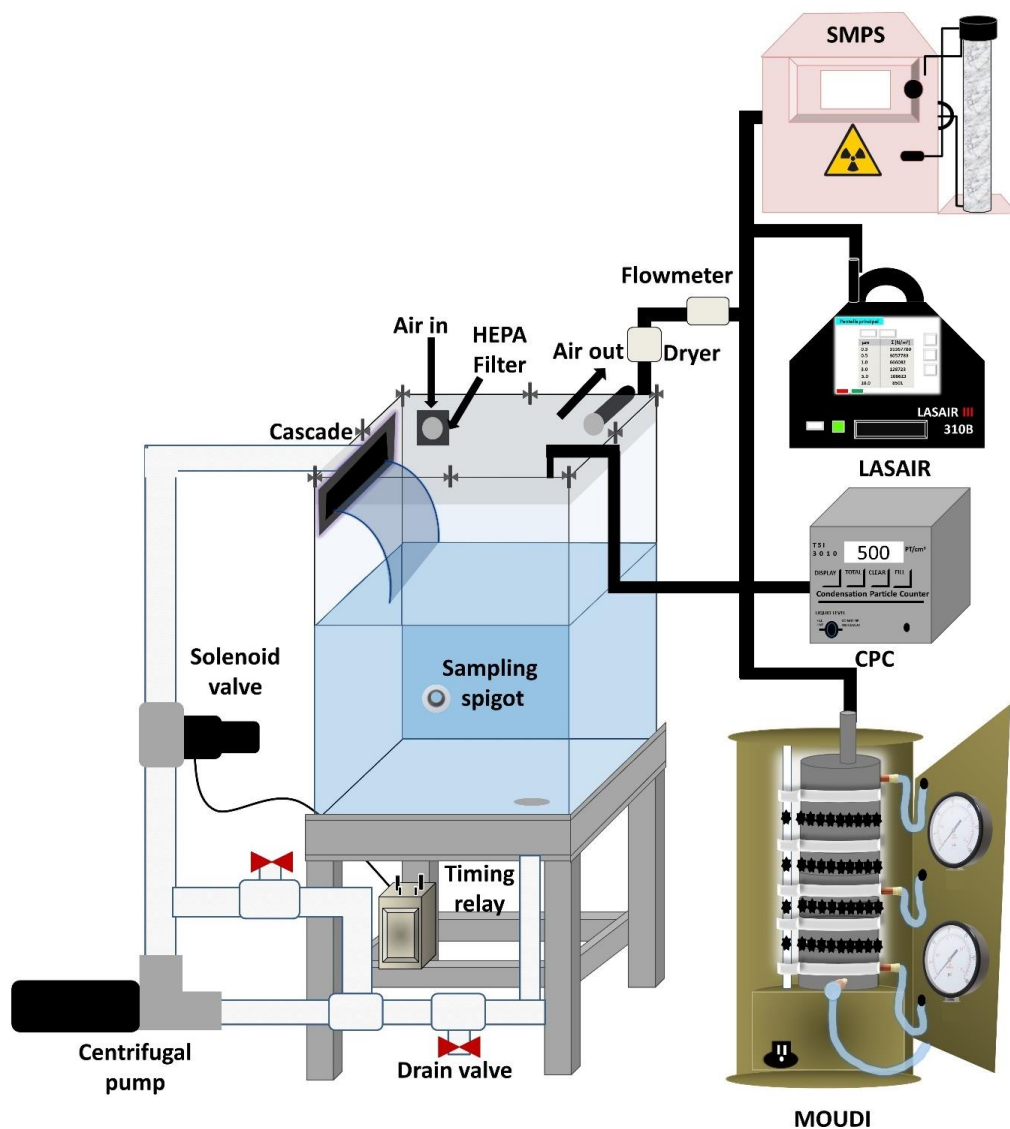
169 The UNAM - MARine Aerosol Tank (UNAM-MARAT) was built based on the design of
170 Stokes et al. (2013) to study the physicochemical properties of SSA and its ability to nucleate
171 ice under controlled conditions in the laboratory, using samples obtained from the oceanic
172 waters that surround Mexico.

173 The UNAM-MARAT consists of an acrylic tank of 42 cm (length) x 32 cm (width) x 60 cm
174 (height) with a total volume of 80.6 L. The tank has a lid of the same material, and to close
175 the tank, the lid is tightened with ten screws; ambient air leaks are prevented by a neoprene
176 O-ring placed between the lid and the tank-body as shown in Figure 1. A waterfall is
177 generated by commercial 30.5 cm long cascade (DYNASTY SpaParts.com), placed at the
178 back of the tank. Other cascades were tested (Sect. 3.2). Given that the tank is typically filled
179 with 40 L of water, the height of the waterfall is about 10 cm from the water. On one side of
180 the tank, a ½" orifice is used as an air intake. Ambient air passes through a high-efficiency
181 particulate filter (HEPA - TSI, # 16020551) for particulate matter $\geq 0.3 \mu\text{m}$ and a black
182 carbon filter (PALL, PN 12011) to retain volatile compounds before entering the tank.
183 Aerosol particles generated in the tank are sampled from the top of the tank through a ¼"
184 orifice. A 1.0" orifice at the bottom of the tank is part of the water circulation system.

185 The circulation system consists of 1.0" internal diameter hoses, PVC pipes, and fittings (Fig.
186 1), a drain valve at the bottom and an on-off valve. The water is pumped with a centrifugal
187 pump (Little Giant PondWorks, model 2-MDQ-SC), and the intermittent automatic water



188 flow is generated and controlled with a corrosion-resistant ½" PVC solenoid valve (WIC
189 VALVE, model 2PCZ-1/2-D-L) and a programmable time-delay relay (Macromatic Relay,
190 Model TR 65122). The water flow is continuously monitored with a flowmeter (GPI TM
191 SERIES, model TM050-N).



192

193 Figure 1. Diagram of the UNAM-MARAT experimental setup and the location of additional
194 instrumentation.



195 Prior to each experiment, the tank is cleaned twice: first with distilled water and then with a
196 mixture of isopropanol and distilled water. The distilled water and the 10% isopropanol
197 solution are recirculated for 30 minutes. This procedure is carried out to eliminate residues
198 and microorganisms from previous experiments. Once the system is cleaned, 10 L of the
199 sample to be used are added to the tank and recirculated for 30 mins to purge it. Subsequently,
200 the tank is completely emptied and filled with 40 L of the water sample to be analyzed. The
201 tank is carefully closed and left to stand overnight. To monitor SSA generation, a
202 condensation particle counter (CPC 3010, TSI) is connected at the inlet located at the top of
203 the tank and data is collected for 20 mins to determine the baseline (background)
204 concentration. Afterward, the waterfall is turned on for 20 minutes to generate aerosol
205 particles, and samples are then taken for 10 minutes. The waterfall operates intermittently to
206 mimic wave breaking (the operating time was 2s on and 10s off).

207 **2.2 Additional instrumentation**

208 Online and offline measurements were made to characterize the SSA generated in the
209 UNAM-MARAT. Due to different flow rates of the online and offline instrumentation, not
210 all instruments sampled simultaneously.

211 SSA PSD for particles larger than 0.3 μm were measured with an optical particle counter
212 (LasAir III 310B, Particle Measuring Systems) with cut sizes of 0.3, 0.5, 1.0, 3.0, 5.0, and 10
213 μm . The data was recorded every 11s and the instrument was operated at a flow rate of 28.3
214 L min^{-1} .

215 SSA PSD for particles ranging between 10 and 400 nm was measured with a Scanning
216 Mobility Particle Sizer (SMPS, TSI). The SMPS setup included an electrostatic classifier
217 (model 3080, TSI), a scanning differential mobility analyzer (DMA, model 3081), and a
218 water condensation particle counter (WCPC, model 3787). The sample flow rate was set at
219 0.6 L min^{-1} . Measurements were taken in 10 consecutive runs, each lasting 5 minutes, while
220 the waterfall was in operation.

221 SSA particles were collected as a function of their aerodynamic diameter using a micro-
222 orifice uniform deposit impactor (MOUDI 100R, MSP) at a flow rate of 29.9 L min^{-1} . The
223 cut sizes of MOUDI are 0.18, 0.32, 0.56, 1.0, 1.8, 3.2, 5.6 and $10.0 \mu\text{m}$ (Mason et al., 2015).
224 Aluminum substrates of 47 mm (TSI) were used for the subsequent chemical composition
225 analysis, while hydrophobic glass coverslips of 22 mm x 22 mm (HR3-215, Hampton
226 Research) were used for the subsequent INP analysis. During a typical experiment, samples
227 were collected four times for 10 mins each, on the same substrate. The substrates were stored
228 in sealed petri dishes at 4°C until analyzed.

229 **2.3 Chemical analysis**



230 Particles collected on the aluminum substrates were analyzed by ion chromatography. The
231 substrates were cut and placed inside polyurethane bottles with 10 mL deionized water, and
232 then placed in an ultrasonic bath (model 3510, Branson) for 1 h at 47°C, allowing for the
233 desorption and fragmentation of organic and inorganic particles. Subsequently, the bottles
234 were placed on a mechanical orbital shaker (model 3005, GFL) for 6 h at 350 rpm. Samples
235 were then filtered with acrodisc syringe filters of 25 mm diameter with a pore size of 0.2 μm
236 (Pall Corporation). Finally, the filtrate was stored at -4°C (Chow and Watson, 1999). The
237 identification and quantification of anions (Cl⁻, NO₃⁻, Br⁻, SO₄²⁻, PO₄³⁻) and cations (Na⁺,
238 Mg²⁺, Ca²⁺, NH₄⁺, K⁺) was performed by a Dionex model ICS-1500 chromatograph equipped
239 with an electrical conductivity detector. A Thermo Scientific Dionex IonPac AS23-4 μm
240 Analytical Column (4 mm x 250 mm) with Thermo Scientific Dionex CES 300 Capillary
241 Electrolytic Suppressor module and the mobile phase was 4.5 mM Na₂CO₃ - 0.8 mM NaHCO
242 at 1 mL min⁻¹ flow rate for anions and a Thermo Scientific Dionex IonPac CS 12A Cation-
243 Exchange Column (4 mm x 250 mm) with the Thermo Scientific Dionex CES 300 Capillary
244 Electrolytic Suppressor and the mobile phase was a solution of CH₄SO₃ 20 mM and 1 mL
245 min⁻¹ flow rate for cations as described in Ladino et al. (2019).

246 The ice nucleation abilities, via immersion freezing, of the SSA particles were measured
247 through the droplet freezing technique (DFT). Detailed information on the operation of the
248 UNAM-DFT can be found in Córdoba et al. (2021); therefore, only a brief description is
249 provided below. The UNAM-DFT consists of four modules: (i) a cold stage, (ii) a humid/dry
250 air system, (iii) an optical microscope with a video recording system, and (iv) a data
251 acquisition system. Each glass coverslip with the SSA is placed on the cold stage and isolated
252 from the ambient atmosphere. Humid air is circulated through the system, inducing liquid
253 droplet formation by water vapor condensation. When droplets reach a diameter of 170 μm
254 (on average), dry air is injected to induce evaporation and to increase the distance between
255 droplets and, hence, to avoid contact droplet freezing. The humid/dry air system and the
256 valves of the cold stage are then closed, and the temperature of the sample holder is decreased
257 from 0 to -40 °C at a cooling rate of 10 °C min⁻¹. Droplet freezing is detected when the droplet
258 changes from bright to opaque as seen during the video analysis. Thus, the freezing
259 temperature is determined through the data acquisition system.

260 The ice-active surface site density (n_s) was derived from Eq. (1) at -15, -20, -25, and -30°C
261 following Si et al. (2018):

$$262 \quad n_s(T) = \frac{[INP(T)]}{S_{tot}} \quad (1)$$

263 where $[INP(T)]$ is the INP concentration (L⁻¹) at temperature (T) and S_{tot} is the total surface
264 area of all aerosol particles. Full details of the n_s calculation can be found in the Supporting
265 Information.



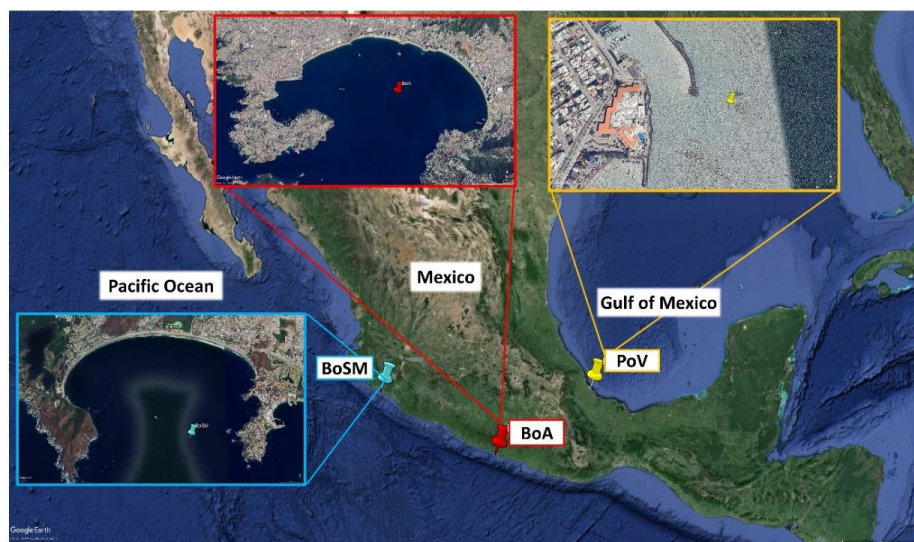
266 The $[INP(T)]$ is obtained from Eq. (2) in Mason et al. (2015):

$$267 \quad [INP(T)] = -\ln\left(\frac{N_u(T)}{N_o}\right) \cdot \left(\frac{A_{deposit}}{A_{DFT}V}\right) \cdot N_o \cdot f_{ne} \cdot f_{nu,0.25-0.10\text{ mm}} \cdot f_{nu,1\text{ mm}} \quad (2)$$

268 where $N_u(T)$ is the number of unfrozen droplets at a temperature $T(^{\circ}C)$, N_o is the total number
269 of droplets (dimensionless), $A_{deposit}$ is the total area of the aerosol particles deposited on the
270 MOUDI hydrophobic glass coverslip (cm^2), A_{DFT} is the area of the sample analyzed by the
271 DFT (cm^2), V is the volume of air through the MOUDI (L), f_{ne} is a correction factor to account
272 for the uncertainty associated with the number of nucleation events in each experiment
273 (dimensionless), and f_{nu} is a correction factor to account for changes in particle concentration
274 across each MOUDI sample (dimensionless).

275 **Collection of ocean water samples**

276 The seawater samples to generate the SSA with the UNAM-MARAT were collected at three
277 different Mexican coastal sites (Figure 2): The Port of Veracruz (PoV, Veracruz), the Bay of
278 Acapulco (BoA, Guerrero), and the Bay of Santiago-Manzanillo (BoSM, Colima). The
279 coordinates are given in Table S1. Approximately 60 L of seawater were collected in 20 L
280 polyethylene containers previously washed with distilled water and purged with seawater.
281 The samples were transported to Mexico City at room temperature. In the case of the BoSM
282 samples, the UNAM-MARAT was deployed to the Water Quality Laboratory located in the
283 University Center for Oceanological Research, University of Colima, Manzanillo, where
284 some experiments were carried out in-situ. A second 60 L of seawater from the BoSM sample
285 was collected (04/09/2022) and transported to Mexico City to evaluate potential changes that
286 may occur during transportation. Before introducing the seawater into the UNAM-MARAT,
287 the samples were filtered with a 50 μm mesh to remove some debris and zooplankton.



288

289 Figure 2. Map showing the sampling locations: The Bay of Acapulco (BoA, red icon), the Port of
290 Veracruz (PoV, yellow icon), and the Bay of Santiago-Manzanillo (BoSM, blue icon). Photo from
291 © Google Earth.

292

293 3 UNAM-MARAT validation

294 3.1 Background particle concentrations

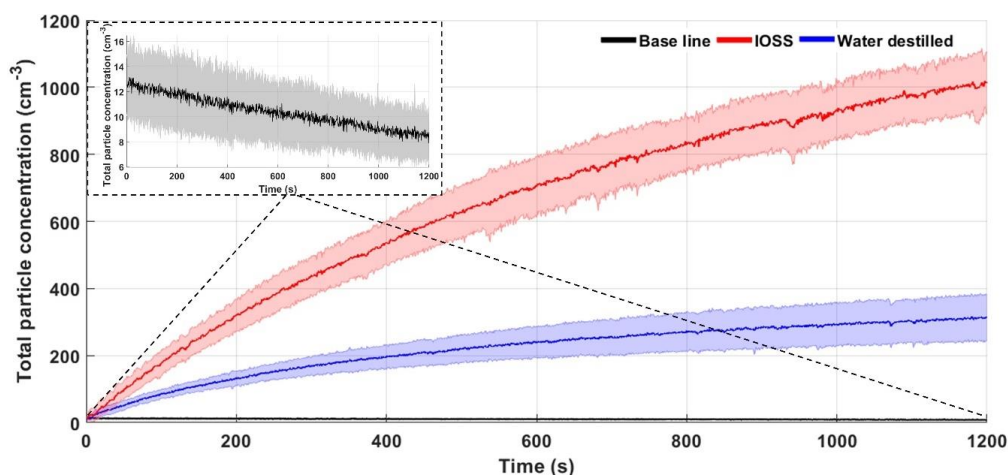
295 Air entering the UNAM-MARAT was filtered to ensure that the measured aerosol particles
296 corresponded solely to those generated by seawater and not due to leaks in the tank. Note
297 that filtered air passing through the CPC resulted in an aerosol concentration of less than 0.1
298 cm^{-3} .

299 Background experiments measured total particle concentrations with the CPC when the tank
300 was filled only with commercial distilled water. An individual experiment consists in
301 measuring the particle concentration for 20 min. This procedure was repeated over three
302 consecutive days, both in the morning and the afternoon (local time). In total, 15 runs were
303 conducted, and the results were averaged with their corresponding standard deviation. Figure
304 3 shows the average particle concentration from the tank when it was filled with distilled
305 water with the cascade off (black line) and with the cascade on (blue line). The shaded areas
306 represent the standard deviation of each curve. The average particle concentration oscillated
307 between 7.8 and $13.2 \pm 2.3 \text{ cm}^{-3}$ with the cascade off (the top left figure shows a zoom of the
308 base line), which indicates that there is a low number of particles within the tank. These
309 results are in accordance with those reported by Prather et al. (2013), who found a baseline
310 $< 20 \text{ cm}^{-3}$ in the Wave Channel. When the cascade was in operation, aerosol particles were



311 generated from the distilled water (up to 313 cm^{-3}), indicating that the water used was not
312 completely free of particles. Also, given that the samples were not passed through a diffusion
313 dryer, it is likely that the measured particles correspond to large water droplets that did not
314 evaporate before entering the CPC.

315 A commercial sea salt (i.e., *Instant Ocean Sea Salt, IOSS*) was used as a proxy for sea water
316 for the validation of UNAM-MARAT. For a typical experiment a solution was prepared in
317 distilled water, achieving a salinity of $28.8 \pm 0.2 \text{ g L}^{-1}$. The tank was filled with 40 L of an
318 IOSS's solution and the total particle concentration was measured with the CPC. The average
319 particle concentration is represented by the red line in Figure 3. It shows that the maximum
320 concentration observed after 20 min of turning on the cascade was 1016 cm^{-3} . Figure 3
321 demonstrates that the UNAM-MARAT is capable of generating SSA, as indicated by the
322 observed increasing concentration.



323

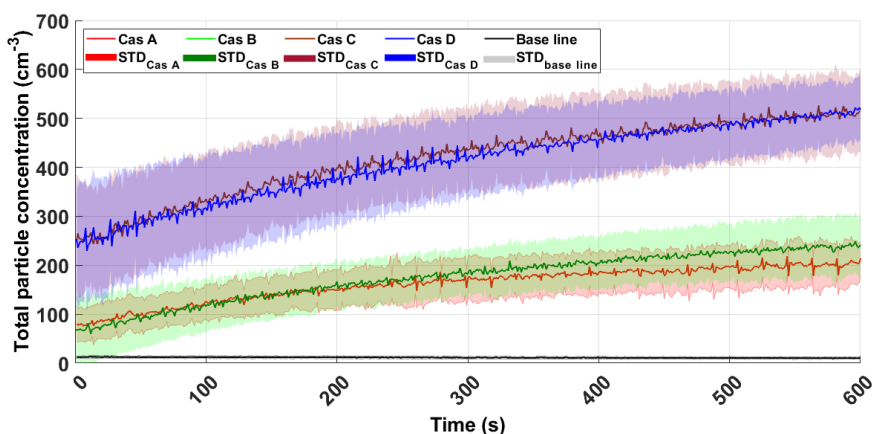
324 Figure 3. Total aerosol concentration as a function of the time (s) with the cascade off (black line in
325 the inset in the upper panel), with the cascade on with distilled water (blue line) and with an IOSS's
326 solution (red line). The shaded areas represent the standard deviation of each curve.

327 3.2 Cascade test

328 To evaluate the role that the cascade plays in SSA generation in the UNAM-MARAT, the
329 tank was filled with 40 L of an IOSS's solution and the total particle concentration was
330 measured when using four different cascades: one was a commercial cascade and the other
331 three were homemade. The homemade waterfalls consisted of cylindrical PVC pipes
332 featuring a slot designed to facilitate the formation of a plunging water sheet. An internal
333 tube with multiple evenly spaced holes was incorporated to enhance water distribution as
334 shown in Figure S1. The main characteristics of each cascade produce with varying slot
335 lengths, inner tube diameters and number of holes, are shown in Table S3.



336 The cascade A produced the lowest particle number concentrations, whereas the highest
337 concentrations were observed with cascades C and D (Fig. 4). As shown in Table S3, the slot
338 length of cascade D is longer than the other cascades, suggesting that the slot's length is a
339 key factor in increasing particle generation.



340

341 Figure 4. Total aerosol number concentration as a function of the time (s) for the different cascades.
342 Each curve represents the average of fourteen experiments, with the shaded area representing the
343 corresponding standard deviation.

344 In contrast, experimental results suggest that the number of holes in the inner cascade tube,
345 and its diameter, play a secondary role in particle production. A longer slot length results in
346 a larger artificially generated wave, through the plunging sheet of water mechanism rather
347 than the plunging jet mechanism.

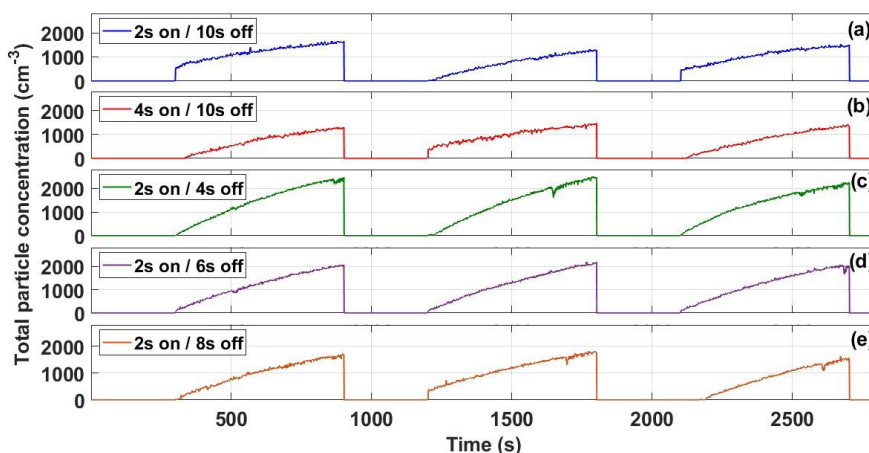
348 Stokes et al. (2013) noted that the shape and penetration of water drops (i.e., plunging sheet
349 or plunging jet) affect aerosol particle production, with plunging sheet generating more
350 particles. In contrast, other aerosol generation systems used in marine tanks have shown
351 limited efficiency, as they often produce particles within a narrow size range. For instance,
352 Fuentes et al. (2010) observed that systems employing glass frits and aquarium diffusers can
353 produce high concentrations of particles, but these particle size typically range between 0.012
354 and 0.018 μm . This limitation arises because these systems primarily simulate the film drop
355 mechanism. Plunging sheet systems, such as in the UNAM-MARAT, can produce a broader
356 range of particles sizes, as they facilitate both the film and jet drop mechanisms, leading to
357 more diverse aerosol size distributions (Stokes et al., 2013)

358 3.3 The intermittency time

359 Waves in marine environments are not generated continuously, mainly due to the different
360 energy processes that drive them, their intensity, and physical and physiographic aspects,
361 resulting in an intermittent behavior (Jelley, 1989). Wang et al. (2017) revealed that a



362 continuous cascade complicates the rupture of bubbles on the water surface, similarly
363 affecting the formation of aerosol particles through the jet drops mechanisms, which is
364 important in generating supermicron particles. For this reason, the solenoid valve controls
365 the intermittence of the cascade and the operating time is modulated with a time-delay relay.
366 Five intermittency values were evaluated: 2 s on / 10 s off, 4 s on / 10 s off, 2 s on / 4 s off,
367 2 s on / 6 s off, and 2 s on / 8 s off. The highest particle concentrations were observed for the
368 2 s on / 4 s off ($\sim 2400 \text{ cm}^{-3}$, Figure 5c) and 2 s on / 6 s off ($\sim 2000 \text{ cm}^{-3}$, Figure 5d)
369 configurations, followed by the 2 s on / 8 s off ($\sim 1600 \text{ cm}^{-3}$, Figure 5e). For the 2 s on / 10 s
370 off (Figure 5a), 4 s on / 10 s off (Figure 5b) configurations, the maximum aerosol
371 concentrations were very similar (about 1400 cm^{-3} after 600 s). Harb and Foroutan, (2019)
372 also evaluated the role of the intermittency (i.e., 3 s on and 1 s off, 3 s on and 2 s off, 3 s on
373 and 3 s off, 3 s on and 4 s off, and 3 s on and 5 s off). The authors conclude that using a
374 longer pause time to allow the bubble plume to develop, is beneficial for facilitating the
375 mechanisms of film and jet drops production. Although the 2 s on / 10 s off configuration did
376 not report the highest particle concentration in the UNAM-MARAT, in the remainder
377 experiments we choose this configuration to be comparable to the configuration used in
378 Stokes et al. (2013). Additionally, using configurations 2 s on / 4 s off and 2 s on / 6 s off
379 tend to create a more continuous plunging sheet, which could affect the size of the aerosol
380 particles produced and may not accurately simulate the natural wave breaking processes.



381

382 Figure 5. Total aerosol number concentration as a function of the time (s). The time series represent
383 experiments with different intermittency values evaluated from an IOSS's solution in the UNAM-
384 MARAT. The different panels correspond to (a) 2 s on 10 s off, (b) 4 s on 10 s off
385 (d), 2 s on 6 s off, and (e) 2 s on 8 s off.

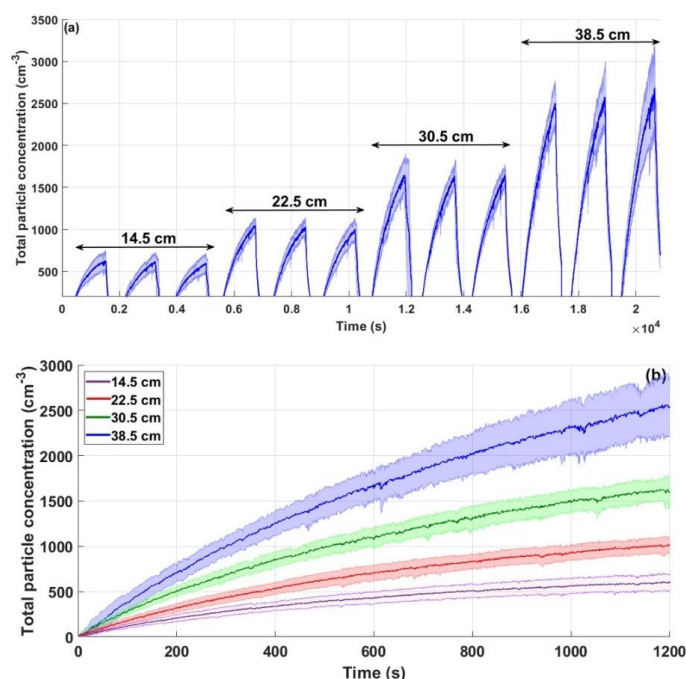
386 Bates et al. (1998) reported that SSA concentrations measured in natural marine
387 environments, such as the Southern Ocean were $< 500 \text{ cm}^{-3}$. Concentrations achieved with
388 the Wave Channel vary between 50 and $100 \text{ particles cm}^{-3}$, while experiments using artificial



389 seawater (i.e., a salt mixture) conducted with the MART have reported particle
390 concentrations ranging from 680 to 1053 cm^{-3} (Thornton et al., 2023). The differences in the
391 concentrations of particles generated in the MART, the Wave Channel, and the UNAM-
392 MARAT tanks can be attributed to several factors, including the aerosol generation
393 mechanism, the composition of the used seawater, and the specific design of each tank. For
394 instance, the Wave Channel uses a paddle to create a disturbance for a wave generation,
395 which affects aerosol production. In contrast, although the MART and the UNAM-MARAT
396 employ similar mechanisms for aerosol generation, the particle concentration differences
397 may be due to the different tank sizes: 210 L (MART) versus 80 L (UNAM-MARAT).

398 3.4 Waterfall height

399 The importance of the waterfall height was assessed by testing different volumes of an
400 IOSS's solution (salinity 28.8 ± 0.2 ppt). The total aerosol number concentration was
401 measured for the following water volumes: 20, 30, 40, and 50 L which resulted in a waterfall
402 height of 38.5, 30.5, 22.5, and 14.5 cm, respectively. Figure 6a shows the average total
403 particle concentration (blue line) with their corresponding uncertainty (shaded area). The
404 experiments for each water volume were performed over three different days.



405

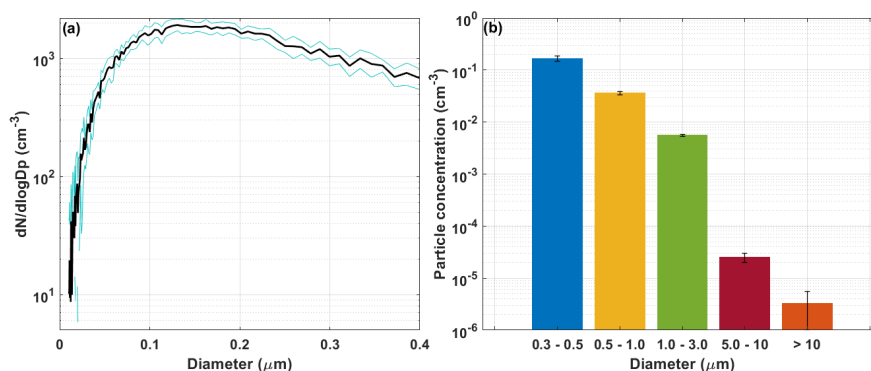
406 Figure 6. Total aerosol concentration as a function of the time (s). (a) the blue line shows the
407 average of three days of repetitions from an IOSS's solution in the UNAM-MARAT. The shaded
408 area represents the uncertainty of those repetitions. (b) Comparison of the average aerosol particle
409 concentrations generated from different volumes with their corresponding uncertainty.



410 The highest concentrations were observed for the largest waterfall height (38.5 cm, 20L of
411 water), with concentrations up to 2500 cm^{-3} , followed by the waterfall height 30.5 cm (30 L
412 of water), which reported a maximum concentration of 1600 cm^{-3} . The lowest concentration
413 (600 cm^{-3}) were recorded for the waterfall height 14.5 cm (50 L of water). Notably, the
414 uncertainty was low at the beginning of the experiments but increased over time (Figure 6b).
415 Although the concentrations for the waterfall height 22.5 cm (40 L of water) were not as high
416 as those reported for the waterfall height 38.5 cm, the uncertainty remained lower throughout
417 the aerosol particle emission process. Therefore, this height was selected for most of the
418 following experiments.

419 3.5 Particle size distribution

420 The final step in characterizing the UNAM-MARAT was to evaluate the PSD of the
421 generated SSA. The particle monitoring was conducted using a SMPS and a LasAir, to assess
422 if the UNAM-MARAT could generate particles across a wide size range. The tank was filled
423 with 40 L of an IOSS's solution and ten experiments were carried out using the intermittent
424 cascade (2 s on, 10 s off). Figure 7a shows the PSD obtained with the SMPS for particles
425 ranging between 10 nm and 400 nm. The black line represents the average of the ten
426 experiments, and the area between the blue lines indicates the standard deviation. A peak in
427 concentration for particles between 0.1 and 0.2 μm in diameter was observed, corresponding
428 to the accumulation mode. This mode is consistent with data reported using the MART
429 (Stokes et al., 2013). The PSD obtained with the LasAir for particles ranging between 300
430 nm and 10 μm is presented in Figure 7b. The highest concentration was observed in the size
431 bin corresponding to the smallest particles (i.e., 0.3 – 0.5 μm). These results demonstrate that
432 the UNAM-MARAT can generate marine aerosol particles with sizes ranging from 30 nm to
433 10 μm .



434

435 Figure 7. Aerosol particle size distribution obtained with the IOSS solution using (a) the SMPS and
436 (b) the LasAir.

437



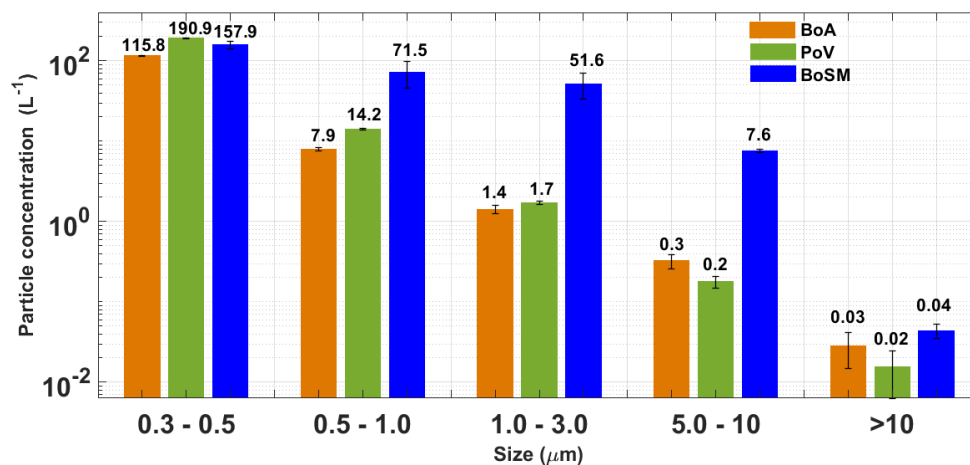
438 **4 Case Study: Ice nucleating abilities of SSA**

439 **4.1 Aerosol particle concentrations and PSD**

440 This section presents the results obtained after generating SSA in the UNAM-MARAT using
441 water samples from BoA, PoV, and BoSM. The results from BoSM correspond to samples
442 collected on April 9, 2022, which were transported to Mexico City, as was the case with the
443 BoA and PoV samples. The SSA generation experiments were performed on April 25, 2022.
444 The highest number of particles generated with the UNAM-MARAT were obtained from the
445 BoSM samples, showing concentrations up to 2000 cm^{-3} . In contrast, the lowest
446 concentrations were observed from the PoV samples (570 and 590 cm^{-3}). This variation
447 related to the origin of the samples may be due to differences in composition (inorganic and
448 organic matter), as the equipment used to generate the SSA was the same and the protocol
449 followed was identical. It is worth noting that at the time of collecting the BoSM samples,
450 the water appeared very turbid, likely due to the decomposition of organic matter. In
451 comparison, the BoA and PoV samples had a clearer appearance.

452 Mayer et al. (2020) reported particle concentrations ranging from 400 to 500 cm^{-3} in an
453 experiment with seawater collected at Scripps Pier, to which nutrients were added to promote
454 phytoplankton blooms. Thornton et al. (2023) emphasize the importance of seawater
455 composition in particle concentration. The authors conducted experiments in the MART,
456 creating mesocosms with the *Thalassiosira weissflogii* diatom and the *Synechococcus*
457 *elongatus* cyanobacterium, observing particle concentrations ranging from 1×10^6 to 2×10^6
458 cm^{-3} for both species, with peaks reaching up to $6 \times 10^6 \text{ cm}^{-3}$.

459 The PSD (for particles larger than 300 nm) from the different samples were comparable as
460 shown in Figure 8. The highest concentrations were observed for particles in the smallest
461 size bin i.e., 0.3 and $0.5 \mu\text{m}$. Out of the three samples, the highest concentrations were
462 observed in the BoSM samples for particles with diameters between 0.5 and $10 \mu\text{m}$ and in
463 the PoV samples for particles between 0.3 and $0.5 \mu\text{m}$. The numbers at the top of the bars in
464 Figure 8 correspond to the average concentrations. Figure 8 also shows that the UNAM-
465 MARAT can produce coarse-mode particles ($> 1 \mu\text{m}$). Generally, particles in this size
466 correspond to sea salt (NaCl) and biological particles (intact or fragmented cells of bacteria,
467 phytoplankton, macrogels, and transparent exopolymer particles, TEP) (Prather et al., 2013;
468 Verdugo et al., 2004). Given that the most efficient INPs are likely particles $> 500 \text{ nm}$
469 (DeMott et al. 2010), the PSD for the ambient samples was only monitored using the LasAir
470 (particles $> 300 \text{ nm}$).

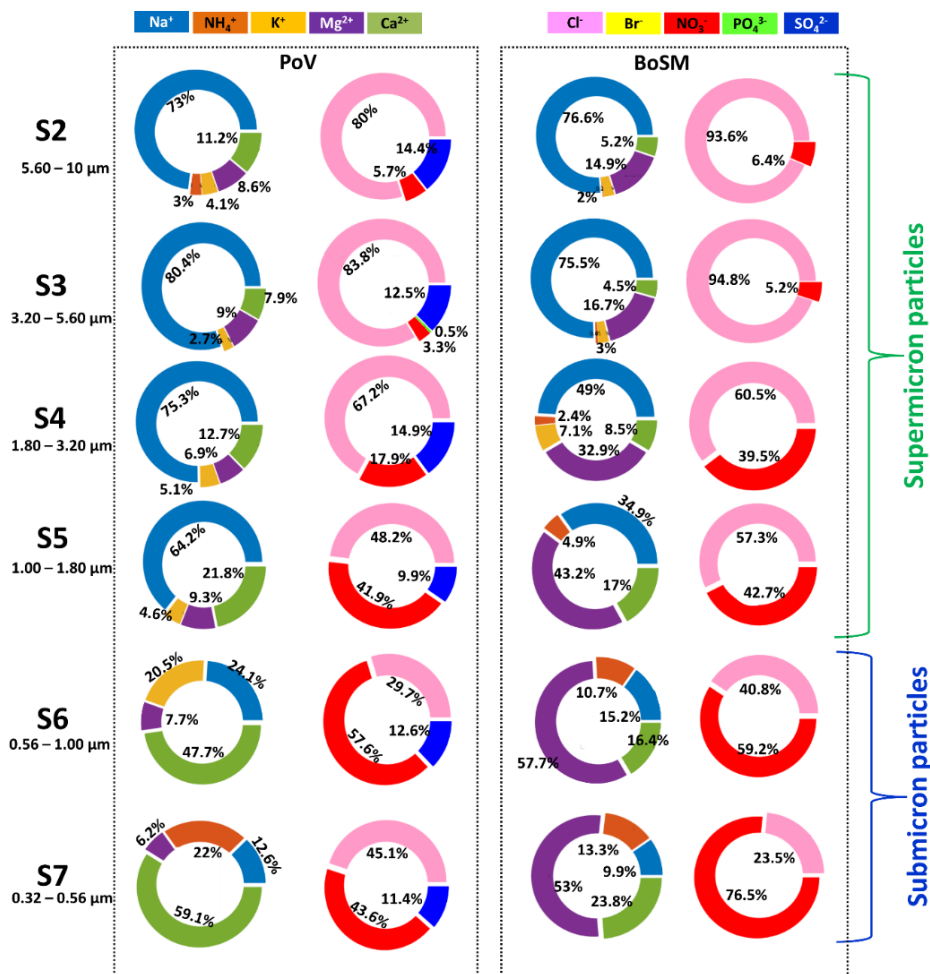


471

472 Figure 8. Aerosol particle size distribution for BoA (orange bars), PoV (green bars), and BoSM
473 (blue bars). The error bars represent the standard deviation for each size bin.

474 4.2 Chemical composition

475 To understand the differences in the chemical composition between samples, the
476 concentration of ions as a function of particle size was analyzed for the PoV and BoSM
477 samples (Figure 9). The BoA sample could not be processed for this specific analysis due to
478 unintentional technical issues. As expected, the dominant ions were Na⁺ and Cl⁻ in both
479 samples. Their concentration was highest for the largest particles (5.6 to 10 μm) and it was
480 lowest for the smallest sizes (0.32- 0.56 μm). An opposite trend was observed for Ca²⁺ and
481 Mg²⁺, as their concentration increases with the particle size. Generally, Ca²⁺ and Mg²⁺ can
482 interact with organic compounds such as carbohydrates, proteins, and lipids. Chin et al.
483 (1998) demonstrated that a proportion of exopolymers present in seawater can assemble into
484 gels through the chelation of Ca²⁺ and Mg²⁺, which form bridges between adjacent or
485 different dissolved organic carbon (DOC) chains.



486

487 Figure 9. Ion concentration (mg L^{-1}) for each MOUDI stage for water samples collected in PoV (left
 488 panel), and BoSM (right panel). The pie charts on the left of each group represent cations, while
 489 those on the right represent anions.

490 Regarding the other ions, NO_3^- showed a similar behavior as Ca^{2+} and Mg^{2+} , while NH_4^+
 491 increases with size from stage 4 (particle size: 1.80 - 3.20 μm) to stage 7 (particle size: 0.32
 492 - 0.56 μm) for the BoSM sample. The presence of ions such as NO_3^- and NH_4^+ may be due
 493 to the decomposition of organic matter or excretions of phytoplankton and zooplankton as
 494 well as the availability of nutrients in the environment of terrigenous origin by runoff or
 495 continental wind input (Anderson et al., 2002). The presence of SiO_4^{2-} in the PoV sample
 496 may be the result of the dissolution of minerals rich in silicates of continental origin or of the
 497 dissolution of ortho silicic acid (H_4SiO_4) that is used in the biogeochemical cycle that is also

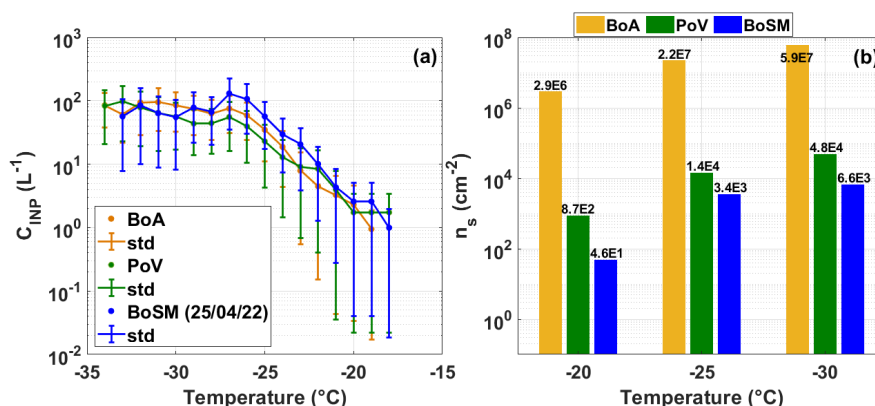


498 regulated by phytoplanktonic and zooplankton organisms (Kuuppo et al., 1998; Wu and
499 Chou, 2003).

500 Bigg and Leck (2008) showed that particles with diameters smaller than 200 nm were
501 exopolymers produced by bacteria and algae, as well as microgels formed from these
502 exopolymers in laboratory experiments. Furthermore, the chemical composition of these
503 particles is closely linked to biological activity. For instance, Facchini et al. (2008)
504 demonstrated that submicron particles collected in the eastern North Atlantic off the coast of
505 Ireland were predominantly composed of organic constituents. Russell et al. (2010) found
506 that the majority of the organic components in submicron aerosol particles collected in the
507 Arctic consisted of organic hydroxyl groups (including polyols and alcohols) characteristic
508 of saccharides. Similarly, Bates et al. (2012) suggested that the organic mass from aerosol
509 particles collected off the coast of California was composed of carbohydrate-like compounds
510 containing organic hydroxyl groups, alkanes, and amines. Our results demonstrate that
511 supermicron particles are largely dominated by sodium chloride. Additionally, our findings
512 indirectly suggest that submicron particles also contain significant amounts of organic
513 material, consistent with the findings reported by Prather et al. (2013).

514 4.3 INPs

515 Figure 10a shows the concentration of INPs for the three set of samples as a function of
516 temperature. The temperatures at which the different samples were able to nucleate ice, via
517 immersion freezing, were found to be -19 to -34°C, -18 to -34°C, and -18 to -33°C for the
518 BoA, PoV, and BoSM samples, respectively. The measured INP concentration ranged from
519 0.9 to 95.4 L⁻¹ for BoA, 1.7 to 97.5 L⁻¹ for PoV, and 0.9 to 130.7 L⁻¹ for BoSM. From these
520 results, it can be inferred that there are no significant differences in the INPs concentrations
521 among the water samples collected from the three sites.



522

523 Figure 10. Comparison of the ice nucleating abilities between samples. (a) INP concentration as a
524 function of temperature and (b) n_s values as a function of temperature. Yellow, green and blue
525 correspond to the BoA, PoV, and BoSM samples, respectively.



526 In an experiment conducted using the MART with seawater collected near SIO, DeMott et
527 al. (2016) found that the INP concentrations varied between 1×10^{-3} and $1 \times 10^3 \text{ L}^{-1}$, with ice
528 nucleation temperatures ranging from -7 to -30°C . The results observed in the marine aerosol
529 samples generated with the UNAM-MARAT (this study) fall within the range reported by
530 DeMott et al. (2016). Additionally, the findings in this study are consistent with those
531 reported by McCluskey et al. (2017), who found that particles generated in the MART with
532 waters collected near SIO, stimulated to produce phytoplankton blooms, were able to
533 nucleate ice between -7 and -32°C , with INP concentrations ranging from 1×10^{-3} and $1 \times$
534 10^1 L^{-1} . On the other hand, Thornton et al. (2023) reported that aerosol particles generated
535 using the MART from waters containing *Thalassiosira weissflogii* *Synechococcus elongatus*,
536 as previously mentioned, exhibited ice freezing temperatures between -14 and -32°C . DeMott
537 et al. (2016) and Thornton et al. (2023) concluded that the warmer freezing temperatures
538 observed in their experiments coincided with peaks in chlorophyll a (Chl-a) in their
539 mesocosms. In contrast, McCluskey et al. (2017) demonstrated that increases in INPs active
540 between -25 and -15°C lagged behind the peak in Chl-a, suggesting a consistent population
541 of INPs associated with the collapse of phytoplankton blooms. The difference with the
542 experiments conducted using the UNAM-MARAT is that no culture medium was added to
543 induce blooms in our experiments.

544 As mentioned earlier, n_s is a robust and quantitative metric for comparing the ice nucleating
545 abilities of aerosol particles (Holden et al., 2021). Therefore, n_s was calculated for each
546 sample, as shown in Figure 10b. It was found that the highest and lowest n_s values were
547 derived from the BoA and BoSM samples, respectively. Although the BoSM sample had the
548 highest particle concentration among the three analyzed samples (Figure 8), it exhibited the
549 lowest n_s values, indicating that the particles emitted from this water sample have fewer
550 active sites for ice nucleation. DeMott et al. (2016) and McCluskey et al. (2017) report high
551 n_s values on the order of 1×10^5 y $1 \times 10^6 \text{ cm}^{-2}$, respectively, which are consistent with the BoA
552 values found in this study (Table S4).

553 **4.4 Correlation of T_{50} with Ion Concentration**

554 Spearman's correlation coefficients were calculated between the concentration of certain ions
555 (since some could not be determined in specific particles sizes) and the median freezing
556 temperature (T_{50}) to evaluate if the ice nucleation efficiency is associated with organic matter
557 (Figure S2). A better correlation was observed in the BoSM samples than the PoV sample.
558 Moreover, the highest Spearman coefficients were found for the samples collected on the
559 second day at BoSM, when the waters were turbid. Considering that the high concentrations
560 of Ca^{2+} and Mg^{2+} ions are associated with continental particles that promote primary
561 productivity in the coastal zone, their subsequent remineralization could mean that the BoSM
562 sample collected on 04/09/22 was enriched in organic material, which explains the high ice
563 nucleation efficiency observed in this sample.



564 **4.5 Analysis of transport in the Manzanillo seawaters samples.**

565 Additional experiments were carried out with the BoSM samples to evaluate whether the
566 transport of samples from the sampling site to our laboratory located in Mexico City affects
567 the ice nucleating abilities of SSA generated in the UNAM-MARAT. Two water samples
568 were taken in the BoSM. The 09/04/22 BoMS “fresh sample” results refer to experiments
569 conducted on the second day after collection (experiments conducted in the field), and the
570 25/04/22 BoMS “aged sample” results refer to the experiments conducted 15 days after
571 collection (experiments conducted in Mexico City). The sample was not preserved to
572 maintain conditions similar to those applied to the BoA and PoV samples.

573 The particle concentration was higher in the aged sample for the sizes between 0.3 and 1.0
574 μm and those $>10 \mu\text{m}$. However, for particles between 1.0 and 10.0 μm , the highest
575 concentrations were observed on the fresh samples as shown in Figure S3a.

576 Since it was observed that aging impacted the number of particles, the impact of aging on the
577 ice nucleating abilities was also analyzed. The n_s values were calculated for three
578 temperatures (i.e., -20, -25, and -30°C). Figure S3b shows that the n_s values were consistently
579 higher in the aged sample. This could indicate that biological activity continued during the
580 transport of the samples, which might explain the increase in n_s values. However, ion
581 concentrations did not change significantly between the fresh and aged samples. It is
582 advisable to perform other chemical analyses to validate this hypothesis.

583 **5 Conclusions**

584 The UNAM-MARAT was specifically designed to simulate waves breaking to generate sea
585 spray aerosol and to evaluate the ability of marine aerosol particles to act as INP. The ideal
586 conditions established to work with the UNAM-MARAT were to use 40 L of seawater in the
587 tank, employ a cascade with a slot length of 28.3 cm, and a plunging sheet intermittent
588 cascade with an operating configuration of 2 s on and 10 s off to achieve particle
589 concentrations exceeding 1000 cm^{-3} .

590 The UNAM-MARAT has proven to be an effective tool for evaluating and analyzing the
591 physical and chemical properties of SSA from seawater samples collected at various
592 locations. It offers a cost - effective alternative to expensive field campaigns, providing a
593 controlled and reproducible method for simulating natural SSA generation. The results
594 obtained from the UNAM-MARAT during its characterization are comparable to those
595 obtained from other wave tanks, confirming its reliability and suitability for marine aerosol
596 studies.

597 From the case study, we were able to successfully generate marine aerosol in the laboratory
598 using seawater samples from various coastal areas of Mexico. The aerosol reached particle
599 concentrations up to 2000 cm^{-3} across a wide range of particles sizes, from 10 nm to 10 μm .



600 Additionally, our results show that the Mexican oceanic waters contain INP with
601 concentrations up to 130.7 L^{-1} . Among the three seawater samples analyzed, the BoA sample
602 exhibited the highest ice nucleation abilities, based on the ice active site density values
603 measured between -20 and -30°C . Furthermore, our findings reveal a direct relationship
604 between particle size and composition. Larger particles ($>1 \mu\text{m}$) were found to be enriched
605 in NaCl, whereas smaller particles showed an increased fraction of Ca^{2+} , Mg^{2+} , and NO_3^-
606 related to the presence and degradation of organic matter.

607 The development of the UNAM-MARAT device and the comprehensive analysis of aerosol
608 particles from different coastal regions contribute significantly to our understanding of the
609 role of marine aerosol particles in mixed cloud formation and in the regional precipitation
610 patterns. The newly built tank will serve as a valuable tool for future atmospheric and
611 environmental studies.

612 **Data availability.** Data are available upon request to the corresponding author.

613 **Author contributions.** MFC, RC, and LAL designed and built the tank. MFC, GBR, and
614 LAL designed the field campaign and the experiments. MFC, AO, GC, IM, and LAL carried
615 out the field measurements and the collection of ambient samples. MFC, DRR, HAO, and
616 TC performed the chemical analysis. MFC and LAL wrote the paper, with contributions from
617 all coauthors.

618 **Competing interest.** The authors declare that they have no conflict of interest.

619
620 **Acknowledgments.** We thank Gabriel García, Manuel García, Omar López, and Victor
621 García for their invaluable assistance in the construction and maintenance of the UNAM-
622 MARAT. Also, we would like to thank Kenia Villela, Daniela Leal, María Isabel Saavedra,
623 Dalia Aguilar, Eva Salinas, and Leticia Martínez for their assistance with the experiments
624 related to the UNAM-MARAT. This study was financially supported by the PAPIIT
625 IN111120 grant, the CONACYT fellowship for doctoral students, and the Marcos Moshinsky
626 Foundation.

627 **References**

628 Albrecht, B. A.: Aerosols, cloud microphysics, and fractional cloudiness, *Science* (80-.),
629 245, 1227–1230, <https://doi.org/10.1126/science.245.4923.1227>, 1989.

630 Alpert, P. A., Aller, J. Y., and Knopf, D. A.: Ice nucleation from aqueous NaCl droplets with
631 and without marine diatoms, *Atmos. Chem. Phys.*, 11, 5539–5555,
632 <https://doi.org/10.5194/acp-11-5539-2011>, 2011.

633 Anderson, D. M., Glibert, P. M., and Burkholder, J. M.: Harmful Algal Blooms and
634 Eutrophication: Nutrient Sources, Composition, and Consequences, *Estuaries*, 25, 704–726,



- 635 <https://doi.org/10.1007/BF02804901>, 2002.
- 636 Bates, T. S., Kapustin, V. N., Quinn, P. K., Covert, D. S., Coffman, D. J., Mari, C., Durkee,
637 P. A., De Bruyn, W. J., and Saltzman, E. S.: Processes controlling the distribution of aerosol
638 particles in the lower marine boundary layer during the first aerosol characterization
639 experiment (ACE 1), *J. Geophys. Res. Atmos.*, 103, 16369–16383,
640 <https://doi.org/10.1029/97JD03720>, 1998.
- 641 Bates, T. S., Quinn, P. K., Frossard, A. A., Russell, L. M., Hakala, J., Petäjä, T., Kulmala,
642 M., Covert, D. S., Cappa, C. D., Li, S. M., Hayden, K. L., Nuaaman, I., McLaren, R., Massoli,
643 P., Canagaratna, M. R., Onasch, T. B., Sueper, D., Worsnop, D. R., and Keene, W. C.:
644 Measurements of ocean derived aerosol off the coast of California, *J. Geophys. Res. Atmos.*,
645 117, 1–13, <https://doi.org/10.1029/2012JD017588>, 2012.
- 646 Bigg, E. K.: Ice Nucleus Concentrations in Remote Areas, [https://doi.org/10.1175/1520-0469\(1973\)030<1153:incira>2.0.co;2](https://doi.org/10.1175/1520-0469(1973)030<1153:incira>2.0.co;2), 1973.
- 648 Bigg, E. K. and Leck, C.: The composition of fragments of bubbles bursting at the ocean
649 surface, *J. Geophys. Res. Atmos.*, 113, 1–7, <https://doi.org/10.1029/2007JD009078>, 2008.
- 650 Boucher, O., Randall, P., Artaxo, C., Bretherton, G., Feingold, P., Forster, V.-M., Kerminen,
651 Y., Kondo, H., Liao, U., Lohmann, P., Rasch, S. K., Satheesh, S., Sherwood, B. S., and
652 Zhang, X. : Clouds and Aerosols. In: *Climate Change 2013: The Physical Science Basis.*
653 Contribution of Working Group I to the Fifth Assessment Report of the Intergovernmental
654 Panel on Climate Change, edited by: [Stocker, T. F., Qin, D., Plattner, G.-K., Tignor, M.,
655 Allen, S. K., Boschung, J., Nauels, A., Xia, Y., Bex, V., and Midgley, P. M.], Cambridge,
656 United Kingdom and New York, NY, USA, 571, 571–657 pp.,
657 <https://doi.org/10.1017/CBO9781107415324.016>, 2013.
- 658 Burrows, S. M., Hoose, C., Pöschl, U., and Lawrence, M. G.: Ice nuclei in marine air:
659 Biogenic particles or dust?, *Atmos. Chem. Phys.*, 13, 245–267, <https://doi.org/10.5194/acp-13-245-2013>, 2013.
- 661 Burrows, S. M., Ogunro, O., Frossard, A. A., Russell, L. M., Rasch, P. J., and Elliott, S. M.:
662 A physically based framework for modeling the organic fractionation of sea spray aerosol
663 from bubble film Langmuir equilibria, *Atmos. Chem. Phys.*, 14, 13601–13629,
664 <https://doi.org/10.5194/acp-14-13601-2014>, 2014.
- 665 Burrows, S. M., McCluskey, C. S., Cornwell, G., Steinke, I., Zhang, K., Zhao, B.,
666 Zawadowicz, M., Raman, A., Kulkarni, G., China, S., Zelenyuk, A., and DeMott, P. J.: Ice-
667 Nucleating Particles That Impact Clouds and Climate: Observational and Modeling Research
668 Needs, *Rev. Geophys.*, 60, 1–45, <https://doi.org/10.1029/2021RG000745>, 2022.
- 669 Chow, J. C. and Watson, J. G.: Ion Chromatography in elemental analysis of airborne
670 particles, *Elemental Anal. Airborne Part.*, 326, 1999.
- 671 Christiansen, S., Salter, M. E., Gorokhova, E., Nguyen, Q. T., and Bilde, M.: Sea Spray
672 Aerosol Formation: Laboratory Results on the Role of Air Entrainment, Water Temperature,
673 and Phytoplankton Biomass, *Environ. Sci. Technol.*, 53, 13107–13116,



- 674 <https://doi.org/10.1021/acs.est.9b04078>, 2019.
- 675 Cipriano, R. and Blanchard, C.: Bubble and Aerosol Spectra Produced by a Laboratory
676 “Breaking Wave,” *J. Geophys. Res.*, 86, 8085–8092, 1981.
- 677 Collins, D. B., Zhao, D. F., Ruppel, M. J., Laskina, O., Grandquist, J. R., Modini, R. L.,
678 Stokes, M. D., Russell, L. M., Bertram, T. H., Grassian, V. H., Deane, G. B., and Prather, K.
679 A.: Direct aerosol chemical composition measurements to evaluate the physicochemical
680 differences between controlled sea spray aerosol generation schemes, *Atmos. Meas. Tech.*,
681 7, 3667–3683, <https://doi.org/10.5194/amt-7-3667-2014>, 2014.
- 682 Córdoba, F., Ramírez-Romero, C., Cabrera, D., Raga, G. B., Miranda, J., Alvarez-Ospina,
683 H., Rosas, D., Figueroa, B., Sung Kim, J., Yakobi-Hancock, J., Amador, T., Gutierrez, W.,
684 Garcia, M., Bertram, A. K., Baumgardner, D., and Ladino, L. A.: Measurement report : Ice
685 nucleating abilities of biomass burning , African dust , and sea spray aerosol particles over
686 the Yucatán Peninsula, *Atmos. Chem. Phys.*, 21, 4453–4470, [https://doi.org/10.5194/acp-21-](https://doi.org/10.5194/acp-21-4453-2021)
687 4453-2021, 2021.
- 688 DeMott, P. J., Hill, T. C. J., McCluskey, C. S., Prather, K. A., Collins, D. B., Sullivan, R. C.,
689 Ruppel, M. J., Mason, R. H., Irish, V. E., Lee, T., Hwang, C. Y., Rhee, T. S., Snider, J. R.,
690 McMeeking, G. R., Dhaniyala, S., Lewis, E. R., Wentzell, J. J. B., Abbatt, J., Lee, C., Sultana,
691 C. M., Ault, A. P., Axson, J. L., Martinez, M. D., Venero, I., Santos-Figueroa, G., Stokes, M.
692 D., Deane, G. B., Mayol-Bracero, O. L., Grassian, V. H., Bertram, T. H., Bertram, A. K.,
693 Moffett, B. F., and Franc, G. D.: Sea spray aerosol as a unique source of ice nucleating
694 particles, *Proc. Natl. Acad. Sci. U. S. A.*, 113, 5797–5803,
695 <https://doi.org/10.1073/pnas.1514034112>, 2016a.
- 696 DeMott, P. J., Hill, T. C. J., McCluskey, C. S., Prather, K. A., Collins, D. B., Sullivan, R. C.,
697 Ruppel, M. J., Mason, R. H., Irish, V. E., Lee, T., Hwang, C. Y., Rhee, T. S., Snider, J. R.,
698 McMeeking, G. R., Dhaniyala, S., Lewis, E. R., Wentzell, J. J. B., Abbatt, J., Lee, C., Sultana,
699 C. M., Ault, A. P., Axson, J. L., Diaz Martinez, M., Venero, I., Santos-Figueroa, G., Stokes,
700 M. D., Deane, G. B., Mayol-Bracero, O. L., Grassian, V. H., Bertram, T. H., Bertram, A. K.,
701 Moffett, B. F., and Franc, G. D.: Sea spray aerosol as a unique source of ice nucleating
702 particles, *Proc. Natl. Acad. Sci.*, 113, 5797–5803, <https://doi.org/10.1073/pnas.1514034112>,
703 2016b.
- 704 Facchini, M. C., Rinaldi, M., Decesari, S., Carbone, C., Finessi, E., Mircea, M., Fuzzi, S.,
705 Ceburnis, D., Flanagan, R., Nilsson, E. D., de Leeuw, G., Martino, M., Woeltjen, J., and
706 O’Dowd, C. D.: Primary submicron marine aerosol dominated by insoluble organic colloids
707 and aggregates, *Geophys. Res. Lett.*, 35, <https://doi.org/10.1029/2008GL034210>, 2008.
- 708 Fall, R. and Schnell, R. C.: Association of an ice-nucleating pseudomonad with cultures of
709 the marine dinoflagellate, *Heterocapsa niei.*, *J. Mar. Res.*, 43, 257–265,
710 <https://doi.org/10.1357/002224085788437370>, 1985.
- 711 Fuentes, E., Coe, H., Green, D., de Leeuw, G., and McFiggans, G.: Laboratory-generated
712 primary marine aerosol via bubble-bursting and atomization, *Atmos. Meas. Tech.*, 3, 141–
713 162, <https://doi.org/10.5194/amt-3-141-2010>, 2010.



- 714 Harb, C. and Foroutan, H.: A Systematic Analysis of the Salinity Effect on Air Bubbles
715 Evolution: Laboratory Experiments in a Breaking Wave Analog, *J. Geophys. Res. Ocean.*,
716 124, 7355–7374, <https://doi.org/10.1029/2019JC015337>, 2019.
- 717 Hartery, S., MacInnis, J., and Chang, R. Y. W.: Effect of Sodium Dodecyl Benzene Sulfonate
718 on the Production of Cloud Condensation Nuclei from Breaking Waves, *ACS Earth Sp.*
719 *Chem.*, 6, 2944–2954, <https://doi.org/10.1021/acsearthspacechem.2c00230>, 2022.
- 720 Hill, T. C. J., Demott, P. J., Tobo, Y., Fröhlich-Nowoisky, J., Moffett, B. F., Franc, G. D.,
721 and Kreidenweis, S. M.: Sources of organic ice nucleating particles in soils, *Atmos. Chem.*
722 *Phys.*, 16, 7195–7211, <https://doi.org/10.5194/acp-16-7195-2016>, 2016.
- 723 Holden, M. A., Campbell, J. M., Meldrum, F. C., Murray, B. J., and Christenson, H. K.:
724 Active sites for ice nucleation differ depending on nucleation mode, *Proc. Natl. Acad. Sci.*
725 *U. S. A.*, 118, 1–9, <https://doi.org/10.1073/pnas.2022859118>, 2021.
- 726 Jacobson, M. Z.: Global direct radiative forcing due to multicomponent anthropogenic and
727 natural aerosols, *J. Geophys. Res. Atmos.*, 106, 1551–1568,
728 <https://doi.org/10.1029/2000jd900514>, 2001.
- 729 Jelley, J. V.: Sea waves: their nature, behaviour, and practical importance, *Endeavour*, 13,
730 148–156, [https://doi.org/10.1016/S0160-9327\(89\)80002-X](https://doi.org/10.1016/S0160-9327(89)80002-X), 1989.
- 731 Knopf, D. A., Alpert, P. A., Wang, B., and Aller, J. Y.: Stimulation of ice nucleation by
732 marine diatoms, *Nat. Geosci.*, 4, 88–90, <https://doi.org/10.1038/ngeo1037>, 2011.
- 733 Kuuppo, P., Autio, R., Kuosa, H., Setälä, O., and Tanskanen, S.: Nitrogen, silicate and
734 zooplankton control of the planktonic food-web in spring, *Estuar. Coast. Shelf Sci.*, 46, 65–
735 75, <https://doi.org/10.1006/ecss.1997.0258>, 1998.
- 736 Ladino, L., Raga, G., Alvarez-Ospina, H., Andino-Enríquez, M., Rosas, I., Martínez, L.,
737 Salinas, E., Miranda, J., Ramírez-Díaz, Z., Figueroa, B., Chou, C., Bertram, A., Quintana,
738 E., Maldonado, L., Si, M., and Irish, V.: Ice-nucleating particles in a coastal tropical site,
739 *Atmos. Chem. Phys.*, 19, 6147–6165, <https://doi.org/10.5194/acp-19-6147-2019>, 2019.
- 740 Ladino, L., Juaréz-Pérez, J., Ramírez-Díaz, Z., Miller, L. A., Herrera, J., Raga, G. B.,
741 Simpson, K. G., Cruz, G., Pereira, D. L., and Córdoba, F.: The UNAM-droplet freezing
742 assay: An evaluation of the ice nucleating capacity of the sea-surface microlayer and surface
743 mixed layer in tropical and subpolar waters, *Atmosfera*, 35, 127–141,
744 <https://doi.org/10.20937/ATM.52938>, 2022.
- 745 Lamarre, E. and Melville, W. K.: Air entrainment and dissipation in breaking waves.pdf,
746 *Nature*, 351, 469–472, <https://doi.org/10.1038/351469a0>, 1991.
- 747 Lewis, E. R. and Schwartz, S. E.: Sea Salt Aerosol Production: Mechanisms, Methods,
748 Measurements and Models- A critical Review, American G., Washington, DC, 2004.
- 749 Mason, R. H., Si, M., Li, J., Chou, C., Dickie, R., Toom-Sauntry, D., Pöhlker, C., Yakobi-
750 Hancock, J. D., Ladino, L. A., Jones, K., Leitch, W. R., Schiller, C. L., Abbatt, J. P. D.,
751 Huffman, J. A., and Bertram, A. K.: Ice nucleating particles at a coastal marine boundary



- 752 layer site: correlations with aerosol type and meteorological conditions, *Atmos. Chem. Phys.*,
753 15, 12547–12566, <https://doi.org/10.5194/acp-15-12547-2015>, 2015.
- 754 Mayer, K. J., Wang, X., Santander, M. V., Mitts, B. A., Sauer, J. S., Sultana, C. M., Cappa,
755 C. D., and Prather, K. A.: Secondary Marine Aerosol Plays a Dominant Role over Primary
756 Sea Spray Aerosol in Cloud Formation, *ACS Cent. Sci.*, 6, 2259–2266,
757 <https://doi.org/10.1021/acscentsci.0c00793>, 2020.
- 758 McCluskey, C., Ovadnevaite, J., Rinaldi, M., Atkinson, J., Belosi, F., Ceburnis, D., Marullo,
759 S., Hill, T. C. J., Lohmann, U., Kanji, Z. A., O’Dowd, C., Kreidenweis, S. M., and DeMott,
760 P. J.: Marine and Terrestrial Organic Ice-Nucleating Particles in Pristine Marine to
761 Continentally Influenced Northeast Atlantic Air Masses, *J. Geophys. Res. Atmos.*, 123,
762 6196–6212, <https://doi.org/10.1029/2017JD028033>, 2018.
- 763 McCluskey, C. S., Hill, T. C. J., Malfatti, F., Sultana, C. M., Lee, C., Santander, M. V., Beall,
764 C. M., Moore, K. A., Cornwell, G. C., Collins, D. B., Prather, K. A., Jayarathne, T., Stone,
765 E. A., Azam, F., Kreidenweis, S. M., and DeMott, P. J.: A dynamic link between ice
766 nucleating particles released in nascent sea spray aerosol and oceanic biological activity
767 during two mesocosm experiments, *J. Atmos. Sci.*, 74, 151–166,
768 <https://doi.org/10.1175/JAS-D-16-0087.1>, 2017.
- 769 Melchum, A., Córdoba, F., Salinas, E., Martínez, L., Campos, G., Rosas, I., Garcia, E.,
770 Olivos, A., Raga, G. B., Pizano, B., Silva, M. M., and Ladino, L. A.: Maritime and continental
771 microorganisms collected in Mexico: An investigation of their ice-nucleating abilities,
772 *Atmos. Res.*, 293, 106893, <https://doi.org/10.1016/j.atmosres.2023.106893>, 2023.
- 773 Prather, K. A., Bertram, T. H., Grassian, V. H., Deane, G. B., Stokes, M. D., DeMott, P. J.,
774 Aluwihare, L. I., Palenik, B. P., Azam, F., Seinfeld, J. H., Moffet, R. C., Molina, M. J., Cappa,
775 C. D., Geiger, F. M., Roberts, G. C., Russell, L. M., Ault, A. P., Baltrusaitis, J., Collins, D.
776 B., Corrigan, C. E., Cuadra-Rodriguez, L. A., Ebben, C. J., Forestieri, S. D., Guasco, T. L.,
777 Hersey, S. P., Kim, M. J., Lambert, W. F., Modini, R. L., Mui, W., Pedler, B. E., Ruppel, M.
778 J., Ryder, O. S., Schoepp, N. G., Sullivan, R. C., and Zhao, D.: Bringing the ocean into the
779 laboratory to probe the chemical complexity of sea spray aerosol, *Proc. Natl. Acad. Sci. U.
780 S. A.*, 110, 7550–7555, <https://doi.org/10.1073/pnas.1300262110>, 2013.
- 781 Quinn, P., Collins, D., Grassian, V., Prather, K., and Bates, T.: Chemistry and Related
782 Properties of Freshly Emitted Sea Spray Aerosol, *Chem. Rev.*, 115, 4383–4399,
783 <https://doi.org/10.1021/cr500713g>, 2015.
- 784 Resch, F. and Afeti, G.: Submicron Film Drop Production by Bubbles in Sea Water, *J.
785 Geophys. Res.*, 97, 3679–3683, <https://doi.org/10.1029/91JC02961>, 1992.
- 786 Rosinski, J., Haagenson, P. L., Nagamoto, C. T., and Parungo, F.: Nature of ice-forming
787 nuclei in marine air masses, *J. Aerosol Sci.*, 18, 291–309, [https://doi.org/10.1016/0021-8502\(87\)90024-3](https://doi.org/10.1016/0021-8502(87)90024-3), 1987.
- 789 Rosinski, J., Haagenson, P. L., Nagamoto, C. T., Quintana, B., Parungo, F., and Hoyt, S. D.:
790 Ice-forming nuclei in air masses over the Gulf of Mexico, *J. Aerosol Sci.*, 19, 539–551,
791 [https://doi.org/10.1016/0021-8502\(88\)90206-6](https://doi.org/10.1016/0021-8502(88)90206-6), 1988.



- 792 Russell, L. M., Hawkins, L. N., Frossard, A. A., Quinn, P. K., and Bates, T. S.: Carbohydrate-
793 like composition of submicron atmospheric particles and their production from ocean bubble
794 bursting, *Proc. Natl. Acad. Sci. U. S. A.*, 107, 6652–6657,
795 <https://doi.org/10.1073/pnas.0908905107>, 2010.
- 796 Schnell, R. C.: Ice Nuclei in Seawater, Fog Water and Marine Air off the Coast of Nova
797 Scotia: Summer 1975, *J. Atmos. Sci.*, 34, 1299–1305, 1977.
- 798 Schnell, R. C. and Vali, G.: Freezing nuclei in marine waters, *Tellus*, 27, 321–323,
799 <https://doi.org/10.3402/tellusa.v27i3.9911>, 1975.
- 800 Sellegri, K., Dowd, C. D. O., Yoon, Y. J., Jennings, S. G., and Leeuw, G. De: Surfactants
801 and submicron sea spray generation, *J. Geophys. Res.*, 111, D22215,
802 <https://doi.org/10.1029/2005JD006658>, 2006.
- 803 Si, M., Irish, V. E., Mason, R. H., Vergara-Temprado, J., Hanna, S. J., Ladino, L. A., Yakobi-
804 Hancock, J. D., Schiller, C. L., Wentzell, J. J. B., Abbatt, J. P. D., Carslaw, K. S., Murray, B.
805 J., and Bertram, A. K.: Ice-nucleating ability of aerosol particles and possible sources at three
806 coastal marine sites, *Atmos. Chem. Phys.*, 18, 15669–15685, <https://doi.org/10.5194/acp-18-15669-2018>, 2018.
- 808 Stokes, M. D., Deane, G. B., Prather, K., Bertram, T. H., Ruppel, M. J., Ryder, O. S., Brady,
809 J. M., and Zhao, D.: A Marine Aerosol Reference Tank system as a breaking wave analogue
810 for the production of foam and sea-spray aerosols, *Atmos. Meas. Tech.*, 6, 1085–1094,
811 <https://doi.org/10.5194/amt-6-1085-2013>, 2013.
- 812 Thornton, D. C. O., Brooks, S. D., Wilbourn, E. K., Mirrielees, J., Alsante, A. N., Gold-
813 bouchot, G., Whitesell, A., and Mcfadden, K.: Production of aerosol containing ice
814 nucleating particles (INPs) by fast growing phytoplankton, *Atmos. Chem. Phys. Discuss.*,
815 [preprint], en revisión, <https://doi.org/https://doi.org/10.5194/acp-2022-806>, 2023a.
- 816 Thornton, D. C. O., Brooks, S. D., Wilbourn, E. K., Mirrielees, J., Alsante, A. N., Gold-
817 Bouchot, G., Whitesell, A., and McFadden, K.: Production of ice-nucleating particles (INPs)
818 by fast-growing phytoplankton, *Atmos. Chem. Phys.*, 23, 12707–12729,
819 <https://doi.org/10.5194/acp-23-12707-2023>, 2023b.
- 820 Trueblood, J. V., Wang, X., Or, V. W., Alves, M. R., Santander, M. V., Prather, K. A., and
821 Grassian, V. H.: The Old and the New: Aging of Sea Spray Aerosol and Formation of
822 Secondary Marine Aerosol through OH Oxidation Reactions, *ACS Earth Sp. Chem.*, 3,
823 2307–2314, <https://doi.org/10.1021/acsearthspacechem.9b00087>, 2019.
- 824 Verdugo, P., Alldredge, A. L., Azam, F., Kirchman, D. L., Passow, U., and Santschi, P. H.:
825 The oceanic gel phase: A bridge in the DOM-POM continuum, *Mar. Chem.*, 92, 67–85,
826 <https://doi.org/10.1016/j.marchem.2004.06.017>, 2004.
- 827 Vergara-Temprado, J., Murray, B. J., Wilson, T. W., O’Sullivan, D., Browse, J., Pringle, K.
828 J., Ardon-Dryer, K., Bertram, A. K., Burrows, S. M., Ceburnis, D., Demott, P. J., Mason, R.
829 H., O’Dowd, C. D., Rinaldi, M., and Carslaw, K. S.: Contribution of feldspar and marine
830 organic aerosols to global ice nucleating particle concentrations, *Atmos. Chem. Phys.*, 17,



- 831 3637–3658, <https://doi.org/10.5194/acp-17-3637-2017>, 2017.
- 832 Wang, X., Sultana, C. M., Trueblood, J., Hill, T. C. J., Malfatti, F., Lee, C., Laskina, O.,
833 Moore, K. A., Beall, C. M., McCluskey, C. S., Cornwell, G. C., Zhou, Y., Cox, J. L.,
834 Pendergraft, M. A., Santander, M. V., Bertram, T. H., Cappa, C. D., Azam, F., DeMott, P. J.,
835 Grassian, V. H., and Prather, K. A.: Microbial control of sea spray aerosol composition: A
836 tale of two blooms, *ACS Cent. Sci.*, 1, 124–131, <https://doi.org/10.1021/acscentsci.5b00148>,
837 2015.
- 838 Wang, X., Deane, G. B., Moore, K. A., Ryder, O. S., Stokes, M. D., Beall, C. M., Collins, D.
839 B., Santander, M. V., Burrows, S. M., Sultana, C. M., and Prather, K. A.: The role of jet and
840 film drops in controlling the mixing state of submicron sea spray aerosol particles, *Proc. Natl.*
841 *Acad. Sci. U. S. A.*, 114, 6978–6983, <https://doi.org/10.1073/pnas.1702420114>, 2017.
- 842 Wilson, T. W., Ladino, L. A., Alpert, P. A., Breckels, M. N., Brooks, I. M., Browse, J.,
843 Burrows, S. M., Carslaw, K. S., Huffman, J. A., Judd, C., Kilthau, W. P., Mason, R. H.,
844 McFiggans, G., Miller, L. A., Najera, J. J., Polishchuk, E., Rae, S., Schiller, C. L., Si, M.,
845 Temprado, J. V., Whale, T. F., Wong, J. P. S., Wurl, O., Yakobi-Hancock, J. D., Abbatt, J.
846 P. D., Aller, J. Y., Bertram, A. K., Knopf, D. A., and Murray, B. J.: A marine biogenic source
847 of atmospheric ice-nucleating particles, *Nature*, 525, 234–238,
848 <https://doi.org/10.1038/nature14986>, 2015.
- 849 Wolf, M. J., Goodell, M., Dong, E., Dove, L. A., Zhang, C., Franco, L. J., Shen, C.,
850 Rutkowski, E. G., Narducci, D. N., Mullen, S., Babbitt, A. R., and Cziczo, D. J.: A link
851 between the ice nucleation activity and the biogeochemistry of seawater, *Atmos. Chem.*
852 *Phys.*, 20, 15341–15356, <https://doi.org/10.5194/acp-20-15341-2020>, 2020.
- 853 Wu, J. T. and Chou, T. L.: Silicate as the limiting nutrient for phytoplankton in a subtropical
854 eutrophic estuary of Taiwan, *Estuar. Coast. Shelf Sci.*, 58, 155–162,
855 [https://doi.org/10.1016/S0272-7714\(03\)00070-2](https://doi.org/10.1016/S0272-7714(03)00070-2), 2003.
- 856 Wurl, O., Werner, E., Landing, W. M., and Zappa, C. J.: Sea surface microlayer in a changing
857 ocean - A perspective, *Elem. Sci. Anthr.*, 5, 31, <https://doi.org/10.1525/elementa.228>, 2017.
- 858 Yakobi-Hancock, J. D., Ladino, L. A., and Abbatt, J. P. D.: Review of Recent Developments
859 and Shortcomings in the Characterization of Potential Atmospheric Ice Nuclei: Focus on the
860 Tropics, *Rev. Ciencias*, 17, 15–34, <https://doi.org/10.25100/rc.v17i3.476>, 2014.
- 861